Int. J. Heat Mass Transfer. Vol. 35, No. 12, pp. 3451–3464, 1992
Printed in Great Britain

0017–9310/92 $5.00 + 0.00

Onset of salt-finger convection in anisotropic and inhomogeneous porous media

FALIN CHEN and JAY W. LU
Institute of Applied Mechanics, National Taiwan University, Taipei, Taiwan 10764, Republic of China

(*Received* 15 *July* 1991 *and in final form* 5 *November* 1991)

Abstract—In the experiment of directional solidification of binary solutions, the salt-finger convection is usually found to occur prior to the onset of plume convection. The plume containing cold solute-rich liquid is ejected from the dendritic mushy zone, an anisotropic and inhomogeneous porous medium. The salt-finger convection is accordingly believed to be responsible for the formation of plume convection. In this paper, we seek the relation between the onset of salt-finger and plume convection in the mushy zone by a linear stability analysis. We begin with a general study on the influences of the anisotropic and inhomogeneous permeability, thermal diffusivity, and solute diffusivity on the stability characteristics of salt-finger convection in the porous medium. Based on the results obtained, we consider the salt-finger instability in a real dendritic mushy zone identified from the experiment and find that the onset solute Rayleigh number R_{sm}^{c} of salt-finger convection is invariably much larger than that of plume convection. It is therefore our belief that there is no salt-finger convection in the mush when the plume is initially ejected from the mush.

1. INTRODUCTION

IN THE directional solidification process of the concentrated alloy, there is a dendritic region separating the melt from the pure solid region [1, 2]. The dendritic mushy zone is a porous medium with anisotropic and inhomogeneous permeability, and possibly thermal and solute diffusivities. Since the dendrites are immersed in the melt, the gradients of temperature and composition of the melt may destabilize the nominally motionless rest state, leading to the onset of salt-finger convection. This convective motion was related to the occurrence of freckling and other macrosegregation defects [3, 4]. Although the precise mechanism for the occurrence of freckles is not clearly understood at present, several investigations [3–8], nevertheless, concluded generally that the occurrence of freckles in the metallic alloys is related to the formation of plume convection.

To explicitly pinpoint the conditions for the onset of plume convection during the directional solidification, Chen and Chen [9] systematically carried out a series of NH_4Cl–H_2O experiments and indicated that the critical solute Rayleigh number across the mushy layer (R_{sm}^{c}) for the onset of plume convection lies in the range between 200 and 250. They also reported that salt-finger convection is always observed in the melt region right above the mush in all experiments in which the plume convection may or may not exist; in addition, the convective motion in the mush after the plume convection occurs is not of salt-finger type but a bulk motion due mostly to the plume flow. In the present study, we would theoretically identify the relation between these two possible convections in the mush. Analysis of the convective motion in solidifying alloys is complicated by the fact that the temperature and composition in the mush are related by the equilibrium phase diagram, and by the fact that the phase change gives rise to a moving boundary problem. In this paper, we consider the simpler problem of onset of salt-finger convection in a saturating anisotropic and inhomogeneous porous substrate, in which no solidification effect is considered.

Thermal convection in a porous medium with anisotropic permeability was first considered by Castinel and Combarnous [10] who conducted an experimental and theoretical investigation. Epherre's theoretical work [11] extended the analysis to account for thermal anisotropy. Wooding [12] considered the influences of temperature-dependent viscosity and anisotropic permeability on the size of cells at onset. Kvernvold and Tyvand [13] analyzed the onset and nonlinear development of thermal convection in more general anisotropic porous media. McKibbin [14] conducted an extensive study on the effects of anisotropy on the convective stability of a porous layer. The inhomogeneous effects in terms of permeability and thermal diffusivity on the convective instability in a porous medium were considered by Green and Freehill [15]. For the onset of salt-finger convection in a porous medium, Nield [16] analytically presented the stability characteristics for various boundary conditions in an isotropic and homogeneous porous medium. In the same porous medium, Taunton and Lightfoot [17] made an extension of Nield's analysis to more completely characterize the stability of

NOMENCLATURE

a_m	wavenumber
C_i	coefficients, equation (8)
C_p	specific heat of fluid
d_m	depth of the porous medium
D	differential operator, d/dz
D_i	coefficients, equation (9)
g	gravitational acceleration constant
i	unit vector in x-direction
j	unit vector in y-direction
k	unit vector in z-direction
$\underline{K}$	permeability tensor, equation (5)
$\underline{K}_T$	thermal diffusivity tensor, equation (6)
$\underline{K}_S$	solute diffusivity tensor, equation (7)
K_i	three components of permeability, equation (5)
P	pressure
Q	see equation (22)
R_S	solute Rayleigh number, $g\beta(S_u-S_l)d_m K_3/(\nu\kappa_{S3})$
R_T	thermal Rayleigh number, $g\alpha(T_u-T_l)d_m K_3/(\nu\kappa_{T3})$
S	salinity, total and disturbance quantity
T	temperature, total and disturbance quantity
u	velocity vector
W	vertical components of disturbance velocity.

Greek symbols

α	thermal expansion coefficient
β	solute expansion coefficient
$\eta_i(z)$	functions of permeability variation in different directions
$\eta_{Si}(z)$	functions of solute diffusivity variation in different directions
$\eta_{Ti}(z)$	functions of thermal diffusivity variation in different directions
κ_{Si}	components of solute diffusivity of species in fluid, equation (7)
κ_{Ti}	components of thermal diffusivity of fluid, equation (6)
μ	dynamic viscosity
ν	kinematic viscosity
ρ	density of fluid
ξ	permeability ratio, K_1/K_3
ξ_S	solute diffusivity ratio, κ_{S1}/κ_{S3}
ξ_T	thermal diffusivity ratio, κ_{T1}/κ_{T3}.

Subscripts

b	basic state
l	lower boundary
u	upper boundary
0	reference property
1	horizontal direction
3	vertical direction.

Superscripts

c	critical value
′	differentiation, d/dz.

thermohaline convection. Later Tyvand [18] extended these two analyses to an anisotropic and homogeneous porous medium.

In the present study, we consider the onset of salt-finger convection in an anisotropic and inhomogeneous porous medium, in which no solidification occurs. The porous medium is assumed to be horizontally isotropic and homogeneous but vertically anisotropic and inhomogeneous, which is generally true for the dendritic mushy zone [3–9]. We first compare the calculated results with the existing data and then implement an extensive discussion on the significance of anisotropic and inhomogeneous effects on the stability of salt-finger convection, where the inhomogeneity is assumed to be an exponential function varying with height and the vertical variations of inhomogeneity in both horizontal and vertical components are identical [15]. Finally, the real porous medium identified in the experiment of Chen and Chen [9] is considered to calculate the R_{sm}^c of salt-finger convection, from which we reach the conclusion concerned with the relation between the onset of the plume and salt-finger convection.

2. PROBLEM FORMULATION

We consider a horizontal porous layer of thickness d_m and of horizontally infinite extent. The top and bottom boundaries are rigid walls maintained at different constant temperatures and salinities, both of which are high at the top and low at the bottom. A Cartesian coordinate system is chosen with the origin at the bottom and the z-axis vertically upward. The steady continuity, momentum, energy, and concentration equations are [18], respectively,

$$\nabla\cdot\mathbf{u}=0 \tag{1}$$

$$\mu\mathbf{u}+\underline{K}\cdot\{\nabla P+\rho_0 g[1-\alpha(T-T_0)+\beta(S-S_0)]k\}=0, \tag{2}$$

$$\mathbf{u}\cdot\nabla T=\nabla\cdot(\underline{K}_T\cdot\nabla T), \tag{3}$$

$$\mathbf{u}\cdot\nabla S=\nabla\cdot(\underline{K}_S\cdot\nabla S), \tag{4}$$

in which the Boussinesq approximation is applied to Darcy's law. In considering a horizontally isotropic porous medium, the permeability, thermal diffusivity, and solute diffusivity are diagonal tensors [18];

$$\underline{\mathbf{K}} = K_1\eta_1(z)(\mathbf{ii}+\mathbf{jj}) + K_3\eta_3(z)\mathbf{kk}, \quad (5)$$

$$\underline{\mathbf{K}}_T = \kappa_{T1}\eta_{T1}(z)(\mathbf{ii}+\mathbf{jj}) + \kappa_{T3}\eta_{T3}(z)\mathbf{kk}, \quad (6)$$

$$\underline{\mathbf{K}}_S = \kappa_{S1}\eta_{S1}(z)(\mathbf{ii}+\mathbf{jj}) + \kappa_{S3}\eta_{S3}(z)\mathbf{kk}. \quad (7)$$

The $\eta_i(z)$, $\eta_{Ti}(z)$, and $\eta_{Si}(z)$, $i = 1$ and 3, are arbitrary functions account for vertical inhomogeneities of permeability, thermal diffusivity, and solute diffusivity, respectively; the coefficients K_i, κ_{Ti}, and κ_{Si}, $i = 1$ and 3, are constants. It is noted that the thermal diffusivity is obtained by dividing the thermal conductivity by the volumetric heat capacity of the fluid $(\rho_0 C_p)_f$, where C_p is the specific heat of the fluid. The principal axes of permeability, thermal diffusivity, and solute diffusivity of the porous medium are assumed to be coincident. Since the principle of exchange of instabilities holds for salt-finger convection in either a porous medium [16], an anisotropic porous medium [18], or an inhomogeneous porous medium [15], we accordingly assume that it also holds for the present situation. Thus, the time derivatives will be dropped from the disturbance equations, and hence omitted from (2), (3), and (4).

The boundary conditions are that at the upper boundary $T = T_u$, $S = S_u$, and the vertical velocity vanishes; at the lower boundary $T = T_l$, $S = S_l$, and the vertical velocity vanishes. In the horizontal directions the boundary conditions are taken to be periodic. The steady basic state is quiescent. After applying relevant boundary conditions on (3) and (4), we obtain the basic temperature and salinity distributions, respectively,

$$T_b = C_1 \int \frac{dz}{\eta_{T3}(z)} + C_2, \quad (8)$$

$$S_b = D_1 \int \frac{dz}{\eta_{S3}(z)} + D_2, \quad (9)$$

where C_1, C_2, D_1, and D_2 are arbitrary constants depend upon the boundary conditions as the functions $\eta_{T3}(z)$ and $\eta_{S3}(z)$ are specified. The pressure is hydrostatic and need not be presented here.

We operate on the momentum equation (2) with $\nabla\times(\underline{\mathbf{K}}\cdot\nabla)\times$ and then take the vertical component to eliminate the pressure. To render the equations nondimensional, we choose d_m as the length scale so that the layer is of unit depth. We also choose the characteristic velocity as ν/d_m, temperature as $(T_u - T_l)\nu/\kappa_{T3}$, and salinity as $(S_u - S_l)\nu/\kappa_{S3}$. We then decompose the velocity, temperature, and salinity fields into basic state and disturbance quantities, and linearize the equations for the latter. The nondimensional disturbance equations, written in the same notation as the dimensional (2), (3), and (4) are

$$\left[\frac{\eta_1}{\eta_3}\nabla_2^2 + \frac{1}{\xi}\frac{\partial^2}{\partial z^2}\right]W - \frac{\eta_1'}{\xi\eta_1}\frac{\partial W}{\partial z} = \eta_1[R_m\nabla_2^2 T - R_{sm}\nabla_2^2 S], \quad (10)$$

$$\frac{1}{\eta_{T3}}W = \left[\xi_T\eta_{T1}\nabla_2^2 + \frac{\partial}{\partial z}\left(\eta_{T3}\frac{\partial}{\partial z}\right)\right]T, \quad (11)$$

$$\frac{1}{\eta_{S3}}W = \left[\xi_S\eta_{S1}\nabla_2^2 + \frac{\partial}{\partial z}\left(\eta_{S3}\frac{\partial}{\partial z}\right)\right]S, \quad (12)$$

where $\nabla_2^2 = \partial^2/\partial x^2 + \partial^2/\partial y^2$ is the horizontal Laplacian. The elements of the permeability, thermal diffusivity, and solute diffusivity tensors are scaled according to $\xi = K_1/K_3$, $\xi_T = \kappa_{T1}/\kappa_{T3}$, and $\xi_S = \kappa_{S1}/\kappa_{S3}$. The thermal and solute Rayleigh numbers are, respectively,

$$R_m = g\alpha(T_u - T_l)d_m K_3/(\nu\kappa_{T3}), \quad (13)$$

$$R_{sm} = g\beta(S_u - S_l)d_m K_3/(\nu\kappa_{S3}), \quad (14)$$

which are defined in terms of the vertical permeability K_3, thermal diffusivity κ_{T3}, and solute diffusivity κ_{S3}. The dimensionless boundary conditions at the top and bottom walls are

$$W(1) = T(1) = S(1) = W(0) = T(0) = S(0) = 0. \quad (15)$$

We apply the normal mode expansion of the dependent variables and use D to denote the differential operator d/dz and obtain the eigenvalue problem consisting of the following ordinary differential equations (ODEs):

$$\left[\frac{1}{\xi}D^2 - \frac{\eta_1'}{\xi\eta_1}D - \frac{\eta_1}{\eta_3}a_m^2\right]W = \eta_1 a_m^2[-R_m T + R_{sm}S], \quad (16)$$

$$\left[D^2 + \frac{\eta_{T3}'}{\eta_{T3}}D - \xi_T\frac{\eta_{T1}}{\eta_{T3}}a_m^2\right]T = \frac{1}{\eta_{T3}}W, \quad (17)$$

$$\left[D^2 + \frac{\eta_{S3}'}{\eta_{S3}}D - \xi_S\frac{\eta_{S1}}{\eta_{S3}}a_m^2\right]S = \frac{1}{\eta_{S3}}W. \quad (18)$$

In these final equations, we have nondimensional horizontal wavenumber a_m, which is the separation constant of normal mode expansion. The boundary conditions on the top and the bottom walls are

$$W(1) = T(1) = S(1) = W(0) = T(0) = S(0) = 0. \quad (19)$$

The eigenvalue problem consists of a sixth-order ODE with six boundary conditions. We regard all thermophysical properties of the porous medium as given. For a given stabilizing temperature gradient R_m, we seek the eigenvalues R_{sm} for given a_m. We use a shooting technique based on a hybrid Adams–Backward Difference method to solve this ODE system. An Adams method is used as the family of nonstiff methods, and backward differentiation formulas as the family of stiff methods. The calculation starts at the bottom and ends at the top. For details of the computational procedure, the reader is referred to Chen *et al.* [19].

3. RESULTS AND DISCUSSION

We begin in Section 3.1 with a discussion on the anisotropic effects in which an extention of the work of Tyvand [18] is carried out. The inhomogeneous effects are discussed in Section 3.2. In Section 3.3 an anisotropic and inhomogeneous porous medium identified in Chen and Chen [9] is used to investigate the onset condition for salt-finger convection, then a discussion on the relation between the stabilities of salt-finger and plume convection is given.

3.1. *Anisotropic effects*

In an analysis of the salt-finger instability in anisotropic porous media, Tyvand [18] obtained an exact solution

$$R_{sm}^{c}=\left[1+\frac{\pi^2}{(a_m^c)^2\xi}+\frac{R_m}{(a_m^c)^2\xi_T+\pi^2}\right][(a_m^c)^2\xi_S+\pi^2]. \tag{20}$$

The corresponding critical wavenumber a_m^c is determined by the polynomial

$$Q^4+a_3Q^3+a_2Q^2+a_1Q+a_0=0, \tag{21}$$

where

$$\begin{aligned} Q&=(a_m^c)^2/\pi^2\\ a_3&=2/\xi_S\\ a_2&=\frac{1}{\xi_S^2}-\frac{R_m}{\pi^2}\frac{\xi_T-\xi_S}{\xi_T\xi_S^2}-\frac{1}{\xi\xi_T}\\ a_1&=-\frac{2}{\xi\xi_T\xi_S}\\ a_0&=-\frac{1}{\xi\xi_T\xi_S^2}. \end{aligned} \tag{22}$$

Only positive real roots for Q have physical sense. Tyvand proved that there is only one positive real root and, therefore, there is always only one mode for the onset of salt-finger convection. We calculate the root of Q by Newton–Raphson iteration scheme and obtain the R_{sm}^c and a_m^c for various ξ, ξ_T, ξ_S, and R_m. These results compare excellently with those obtained by our numerical integration. Please note that the definitions of R_m and R_{sm} in (13) and (14), respectively, are different from those in Tyvand by a negative sign.

To illustrate the physical significance of the anisotropies, we use equations (20)–(22) to systematically calculate the R_{sm}^c and a_m^c for $R_m=1$, 50 and $\xi_T=1$, 0.1 in $0.1\leqslant\xi\leqslant 1$ and $0.1\leqslant\xi_S\leqslant 1$. The $R_m=50$ is a reasonable scale for a laboratory setup in which a 3 cm thick porous layer consisting of 3 mm diameter glass beads is immersed in a small concentration salt–water solution. The $R_m=1$ scale, according to the experiment of Chen and Chen [9], is relevant to the thermal gradient across the dendritic mushy layer as the plume convection thresholds. The reason to select only two values of $\xi_T=1$ and 0.1 is that we find the influence of ξ_T on the stability characteristics is much smaller than that of either ξ or ξ_S. The influence of ξ_T, however, becomes more profound as R_m increases. The exact solutions (20)–(22) of aforementioned cases are presented in Figs. 1–3. According to equations (13) and (14), R_m and R_{sm} are defined in terms of the vertical permeability K_3, vertical thermal diffusivity κ_{T3}, and vertical solute diffusivity κ_{S3}. We consider the values of these three properties as fixed in interpreting the physical meaning of the results shown in Figs. 1–3 as well as subsequent relevant figures in this paper. Accordingly, smaller ξ, for example, implies smaller horizontal permeability. The same implication applies for both ξ_T and ξ_S.

For $R_m=1$ and $\xi_T=1$ (Figs. 1(a), (b)), both R_{sm}^c and a_m^c increase with decreasing ξ. Because smaller horizontal permeability inhibits horizontal fluid motion, the motionless state is thus stabilized and therefore R_{sm}^c increases. Since larger resistance to horizontal flow also leads to a shortening of the horizontal critical wavelength, a_m^c accordingly increases with decreasing ξ. In the same figures, one sees that R_{sm}^c increases and a_m^c decreases with increasing ξ_S. Phys-

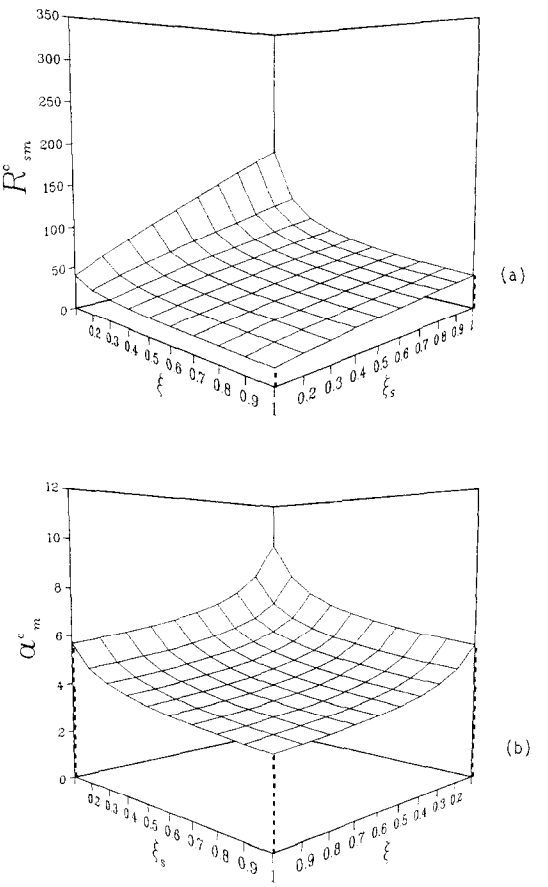

FIG. 1. Anisotropic effects on the critical conditions for $R_m=1$ and $\xi_T=1$. (a) R_{sm}^c; (b) a_m^c.

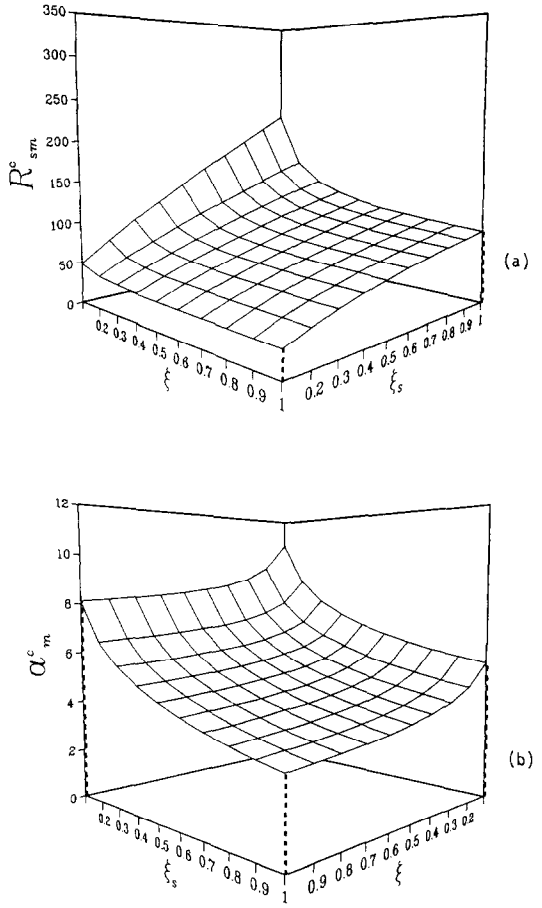

FIG. 2. Anisotropic effects on the critical conditions for $R_m = 50$ and $\xi_T = 1$. (a) R^c_m; (b) a^c_m.

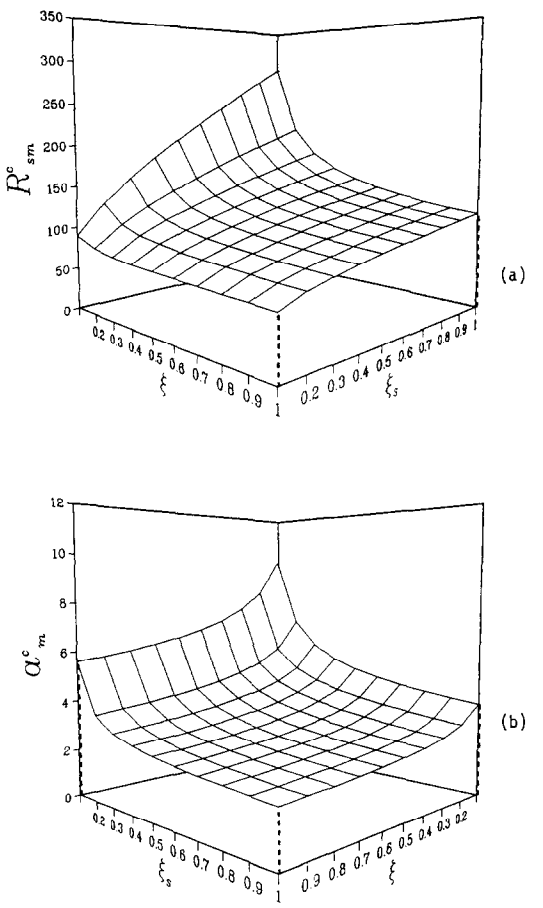

FIG. 3. Anisotropic effects on the critical conditions for $R_m = 50$ and $\xi_T = 0.1$. (a) R^c_m; (b) a^c_m.

ically, this means larger solute diffusivity in horizontal direction corresponds to stabilization of the base state with larger critical wavelength. This can be explained by the fact that as ξ_S increases, the mass contained in a fluid parcel is easier to lose in the horizontal direction, and hence the fluid parcel is easier to homogenize its concentration with ambient fluid and leads to stabilization as well as larger critical wavelength. Note that the increase of stabilization due to the decreases of ξ is about the same with that due to the increase of ξ_S for the present case. Similar conclusion applies for the increase of a^c_m due to both decreasing ξ and ξ_S. We also investigate the case for $\xi_T = 1$ with the same R_m and find that the difference between the results of $\xi_T = 1$ and 0.1 is negligible.

For $R_m = 50$ and $\xi_T = 1$ (Figs. 2(a), (b)), both R^c_{sm} and a^c_m again increase with decreasing ξ. The variations of both these values with ξ for $R_m = 50$ are very close to those for $R_m = 1$. This means the influence of permeability anisotropy on the stability characteristics does not change with different stabilizing thermal gradient. Both the increase of R^c_{sm} and decrease of a^c_m with increasing ξ_S, however, are much larger for $R_m = 50$ than for $R_m = 1$. It is known that larger stabilizing thermal gradient (i.e. larger R_m) needs larger destabilizing solute gradient (i.e. larger R_{sm}) to make the conduction state unstable. The need for larger R_m is enhanced for larger horizontal solute diffusivity because the mass is diffused faster horizontally so that a larger vertical solute gradient is necessary for building up the potential of destabilization. With regard to a^c_m, the decrease of a^c_m with increasing ξ_S is also enhanced for larger R_m, but its physical mechanism of this enhancement is not immediately clear.

In considering the thermal anisotropy of $\xi_T = 0.1$ for $R_m = 50$ (Figs. 3(a), (b)), it is found that the influence of ξ is still the same but the increase of R^c_{sm} and the decrease of a^c_m with increasing ξ_S is reduced compared with those of $\xi_T = 1$, $R_m = 50$. It is known that as ξ_T decreases, a heated fluid parcel loses less heat in the horizontal directions, and hence retains its stabilizing factor better and therefore the base state needs larger destabilizing solute gradient (i.e. larger R^c_{sm}) to lead to destabilization with larger critical wavelength. As a result, the R^c_{sm} in Fig. 3(a) is gen-

erally larger than the corresponding R_{sm}^c in Fig. 2(a) and the a_m^c in Fig. 3(b) is smaller than the corresponding a_m^c in Fig. 2(b).

For convenience in subsequent discussions, we summarize the influence of the anisotropies in the following:

To R_{sm}^c:

1. Decreasing ξ leads to increasing R_{sm}^c—negative effect.
2. Increasing ξ_S leads to increasing R_{sm}^c—positive effect.
3. Decreasing ξ_T leads to increasing R_{sm}^c—negative effect.
4. As far as the cross effect is concerned, the individual effect of each anisotropy will not be changed in trend by the inclusion of the other anisotropic effect. For example, the decreasing variation of R_{sm}^c with increasing ξ will not become an increasing variation when the influence of either ξ_S or ξ_T comes into play. However, a positive anisotropic effect can be enhanced by another positive effect and be reduced by the other negative effect. For instance, the increase of R_{sm}^c with decreasing ξ is enhanced for larger ξ_S but is reduced for larger ξ_T.
5. The rule of cross effect does not apply for the effect of R_m. Note that R_{sm}^c increases with increasing R_m (positive effect). Nonetheless, increasing R_m does not affect the influence of ξ but makes the influences of both ξ_S and ξ_T more profound.

To a_m^c:

1. Decreasing ξ leads to increasing a_m^c—negative effect.
2. Decreasing ξ_S leads to increasing a_m^c—negative effect.
3. Increasing ξ_T leads to increasing a_m^c—positive effect.
4. The cross-effect rule for R_{sm}^c also applies for a_m^c.
5. Larger R_m leads to larger a_m^c, makes no difference on the influence of ξ, leads the influence of ξ_T to be less profound but that of ξ_S more profound.

The above conclusions are reached on the basis of the results for ξ, ξ_T, and ξ_S lying in the range between 0.1 and 1. For the range between 0 and 0.1, these conclusions are also valid [19]. For the range larger than 1, these conclusions generally hold except that the effect of ξ_T may become opposite as inhomogeneous effects are simultaneously considered, which will be discussed in Section 3.3. We note that although (20) may also throw light on the anisotropic effects on R_{sm}^c (but not on a_m^c through equations (21)–(22)) as discussed above, the quantitiative illustrations of these effects as shown in Figs. 1(a)–3(a) are more concrete.

To gain more physical insights into the nature of salt-finger instability in anisotropic porous medium, we present the onset streamline patterns for various ξ, ξ_T, and ξ_S. The streamline patterns are obtained by converting the eigenfunction of perturbed vertical velocity W, which is obtained by the numerical integration of present study. For each streamline plot, the width represents half critical wavelength of the perturbed flow and the height is the thickness of the porous layer. In total eleven streamline plots are shown in Fig. 4. In the first column of plots, the onset convection cells of $R_m = 1$ and $\xi_T = \xi_S = 1$ are presented in Fig. 4(a1) for $\xi = 1$, in Fig. 4(a2) for $\xi = 0.5$, and in Fig. 4(a3) for $\xi = 0.1$. It is seen that the aspect ratio (the height divided by the width) of the cell is larger for smaller ξ since larger horizontal resistance to the flow shortens the horizontal critical wavelength. Please note that only one plot is shown in the first array because they are all identical for $R_m = 1$ and 50 when $\xi = \xi_T = \xi_S = 1$. In the second column, the cells of $R_m = 1$ and $\xi = \xi_T = 1$ are presented in Fig. 4(b2) for $\xi_T = 0.5$ and in Fig. 4(b3) for $\xi_S = 0.1$. It is seen that the decrease of horizontal thermal diffusivity does not considerably influence the cell size for the present case. In the third column, the cells presented are for $R_m = 1$ and $\xi = \xi_T = 1$, where Fig. 4(c2) is for $\xi_S = 0.5$ and Fig. 4(c3) for $\xi_S = 0.1$. As the same with the effect of varying ξ, the decrease in horizontal solute diffusivity (decreasing ξ_S) reduces the critical wavelength. The streamline patterns for $R_m = 50$, $\xi_T = \xi_S = 1$, $\xi = 1$, 0.5, and 0.1 (not shown) are identical with the corresponding ones shown in Figs. 4(a1)–4(a3), respectively, because the increase of stabilizing thermal gradient does not influence the anisotropic permeability effect. We present the onset cell for $R_m = 50$, $\xi = \xi_S = 1$, $\xi_T = 0.5$ and 0.1 in Figs. 4(d2) and 4(d3), respectively. It is seen that larger R_m enhances the increase of critical wavelength due to decreasing ξ_T. Similarly, as shown in Figs. 4(e2) and 4(e3) for $\xi_S = 0.5$ and 0.1, respectively, when $R_m = 50$ and $\xi = \xi_T = 1$, the decrease of critical wavelength due to decreasing ξ_S is also enhanced by increasing R_m. Finally, one notices that the maximum of W always lies at the half height of the layer, the anisotropies of the porous medium influence only the width but not the height of the convection domain.

3.2. *Inhomogeneous effects*

To examine the inhomogeneous effects, we assume in this section that the porous medium is isotropic, i.e. $\xi = \xi_T = \xi_S = 1$. We also assume the vertical variations of inhomogeneity in both the horizontal and vertical directions are exponential functions; in other words, we have

$$\eta_1(z) = \eta_3(z) = e^{Az},$$
$$\eta_{T1}(z) = \eta_{T3}(z) = e^{Bz},$$
$$\eta_{S1}(z) = \eta_{S3}(z) = e^{Cz}. \tag{23}$$

With this assumption, the anisotropies do not change due to the inhomogeneities and vice versa. Accordingly, the inhomogeneous effects do not couple with the anisotropic effects. The assumption of exponential function can be qualitatively justified by the observations of experiments [3, 9]. In equation (23), the

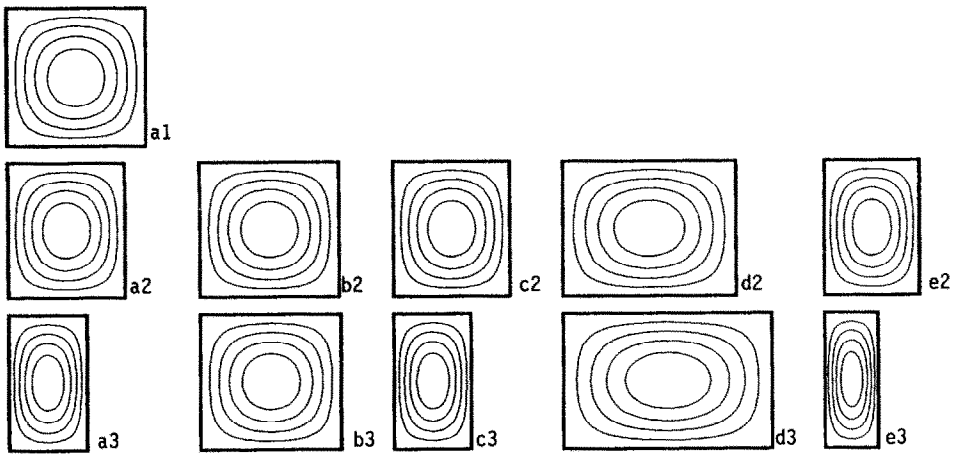

FIG. 4. The streamline patterns in an anisotropic and homogeneous porous layer at selected values of ξ, ξ_T, and ξ_S for $R_m = 1$ and 50. (a1) $\xi = 1$, $\xi_T = \xi_S = 1$, $R_m = 1$; (a2) $\xi = 0.5$, $\xi_T = \xi_S = 1$, $R_m = 1$; (a3) $\xi = 0.1$, $\xi_T = \xi_S = 1$, $R_m = 1$; (b2) $\xi_T = 0.5$, $\xi = \xi_S = 1$, $R_m = 1$; (b3) $\xi_T = 0.1$, $\xi = \xi_S = 1$, $R_m = 1$; (c2) $\xi_S = 0.5$, $\xi = \xi_T = 1$, $R_m = 1$; (c3) $\xi_S = 0.1$, $\xi = \xi_T = 1$, $R_m = 1$; (d2) $\xi_T = 0.5$, $\xi = \xi_S = 1$, $R_m = 50$; (d3) $\xi_T = 0.1$, $\xi = \xi_S = 1$, $R_m = 50$; (e2) $\xi_S = 0.5$, $\xi = \xi_T = 1$, $R_m = 50$; (e3) $\xi_S = 0.1$, $\xi = \xi_T = 1$, $R_m = 50$.

parameters A, B, and C range from zero in homogeneous case to a non-zero value in inhomogeneous case. With the definitions of (23), the inhomogeneous functions are unity at bottom ($z = 0$), increase upwards with z when the parameters are positive and decrease when negative. In addition, for positive parameters, the bulk values of permeability and diffusivities are larger than those of homogeneous case, and vice versa for negative parameters.

The inhomogeneous effects can be categorized as local effect and bulk effect [20]. For the inhomogeneous permeability effect, for instance, as A is largely positive, the local permeability in the upper part of the layer is so large that the onset of convection occurs locally underneath the top boundary and thus reduces the critical wavelength—local effect; for similar A, the overall permeability of the porous layer becomes large that the conduction state is easier to be destabilized and the R_{sm}^c is smaller—bulk effect. In this section, we discuss the bulk effect first by focusing on the single effect due to each of three inhomogeneities for both $R_m = 1$ and 50. Then the local effect is discussed by the illustrations of streamline patterns at the onset.

We first examine each single inhomogeneous effect for $R_m = 1$. The variations of R_{sm}^c and a_m^c with A, B, and C are shown in Figs. 5(a), (b), and (c), respectively. In Fig. 5(a), $B = C = 0$, R_{sm}^c decreases monotonically with increasing A and the increase of a_m^c with $|A|$ is symmetric with respect to $A = 0$. As explained previously, increasing A leads to a less stable state due to the increase of bulk permeability and to a smaller critical wavelength due to local occurrence of the onset of convection (seen in Fig. 7). As regards the effect of inhomogeneous thermal diffusivity (Fig. 5(b)), both R_{sm}^c and a_m^c decrease monotonically with increasing B and reach to be constants of $R_{sm}^c = 4\pi^2$ and $a_m^c = \pi$, respective, with an asymptotic approach. In fact, at $B \approx 1$, R_{sm}^c differs from $4\pi^2$ only by 1% and a_m^c reaches to be π at even smaller B. This means for $B \geqslant 1$ with $R_m = 1$ and $A = C = 0$, the stability characteristics of salt-finger convection (double-diffusive convection) are essentially identical

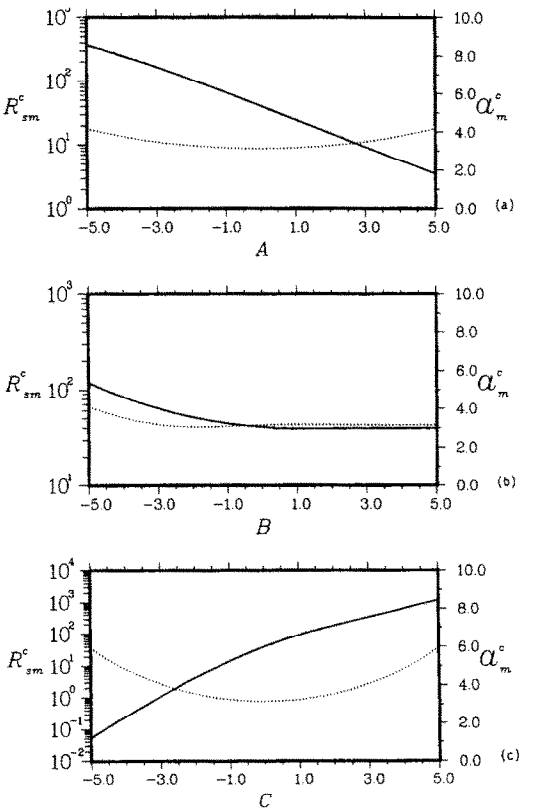

FIG. 5. Inhomogeneous effects on the critical conditions for $R_m = 1$. (a) $B = C = 0$; (b) $A = C = 0$; (c) $A = B = 0$.

with those of thermal convection (single-diffusive convection). Physically, it means that the stabilizing thermal gradient vanishes as B increases to a large enough value because increasingly positive B results in a large bulk thermal diffusivity to homogenize the temperature variation in a short time. Under such a circumstance, the stabilizing thermal gradient disappears and the destabilizing solute gradient serves as the only diffusion agency in the convection so that the stability characteristics of the salt-finger convection are the same with those of thermal convection. It is also found that the critical B^c, at which a souble-diffusive convection becomes a single-diffusive connection, increases with R_m and this will be confirmed later. With regard to the inhomogeneous effect of solute diffusivity (Fig. 5(c)), R^c_{sm} increases monotonically with C and, as that due to varying A, the increase of a^c_m with $|C|$ is symmetric with respect to $C = 0$. The increase of a^c_m due to the variation of C is larger than that due to the variation of A. For $R_m = 50$, the corresponding cases to Figs. 5(a)–(c) are shown in Figs. 6(a)–(c), respectively. In general, the influence of inhomogeneity for $R_m = 50$ is similar in qualitative sense to that for $R_m = 1$. Quantitatively, both R^c_{sm} and a^c_m for $R_m = 50$ are larger than the corresponding ones for $R_m = 1$ except that the variation of a^c_m with A as $B = C = 0$ does not change with R_m. The B^c of $R_m = 50$ is approximately 6.2, which is not shown in Fig. 6(b).

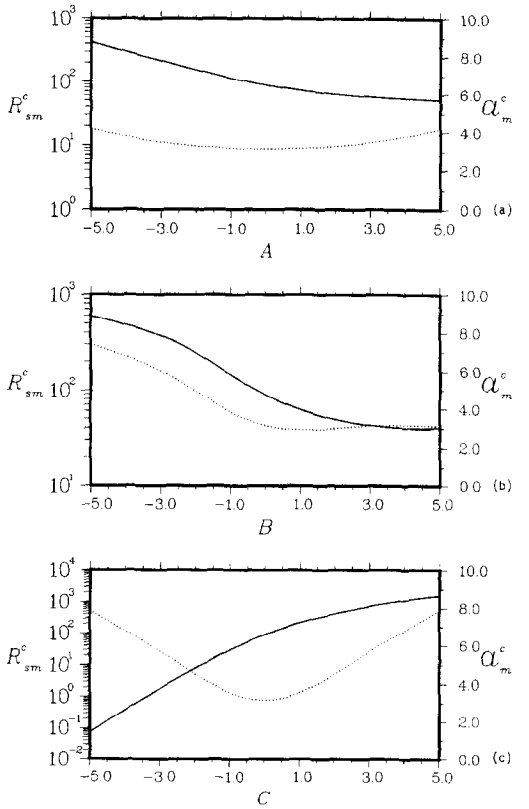

FIG. 6. Inhomogeneous effects on the critical conditions for $R_m = 50$. (a) $B = C = 0$; (b) $A = C = 0$; (c) $A = B = 0$.

To illustrate the local effect due to the inhomogeneities of the porous medium, we present the onset streamline patterns for $R_m = 1$ and 50 in Fig. 7, in which A, B, and C vary from 1 to -1. In the first column, we have the onset cells for $A = 1$, 0, and -1 in Figs. 7(a1), (a2), and (a3), respectively, in which $R_m = 1$ and $B = C = 0$. For $A = 1$, the permeability increases upwards so that the onset of convection occurs locally in the upper part of the layer, where the permeability is larger. For $A = 0$, the porous medium is homogeneous and isotropic so that the cell lies at the middle of the layer. In fact, the plots in the second array of Fig. 7 are all identical because they are the same cases. For $A = -1$, the onset cell occurs in the lower part of the layer where the permeability is larger. As to the inhomogeneous thermal diffusivity effect, the onset cell for $B = 1$ (Fig. 7(b1)) is identical with the homogeneous and isotropic case since B^c is approximately unity for this case. For $B = -1$ (Fig. 7(b3)), the larger thermal diffusivity in lower part of the layer induces more convection because the stabilizing thermal gradient vanishes faster for larger thermal diffusivity so that the convection is easier to set in. In the third column, the onset cells of $C = 1$ and -1 for $R_m = 1$, $A = B = 0$ are shown in Figs. 7(c1) and (c3), respectively. For larger solute diffusivity, the destabilizing solute gradient is easier to be vanished due to larger solutal diffusion so that the onset of convection is easier to threshold in the region of smaller solute diffusivity, and this is the case shown in Figs. 7(c1) and (c3). For $R_m = 50$, the local effects of B and C are obvious as shown by Figs. 7(d1)–(d3) and 7(e1)–(e3), respectively. For stronger stabilizing thermal gradient (i.e. larger R_m), these two effects are enhanced compared with those of $R_m = 1$. The onset cells of $B = C = 0$, $R_m = 50$ (not shown) are identical with those of $R_m = 1$ in Figs. 7(a1)–(a3) since the inhomogeneous permeability effect is not influenced by varying R_m.

As we discussed previously, the salt-finger double-diffusive convection becomes a single-diffusive convection when $B = B^c$, which increases with R_m. To illustrate this change of type of convection more systematically, we present in Fig. 8 several regions in terms of B and R_m. Region 1 is for $R^c_{sm} > (1+10\%)4\pi^2$, region 2 for $(1+5\%)4\pi^2 < R^c_{sm} < (1+10\%)4\pi^2$, region 3 for $(1+1\%)4\pi^2 < R^c_{sm} < (1+5\%)4\pi^2$, and region 4 for $R^c_{sm} < (1+1\%)4\pi^2$, in which the stability characteristics of salt-finger convection are almost identical with those of thermal convection. We thus define the boundary between regions 3 and 4 as the critical boundary, at which the double-diffusive convection becomes the single-diffusive convection in terms of stability characteristics and the B of this curve is named B^c. This figure would provide a clear picture for a quick estimation of the influence of inhomogeneity of thermal diffusivity on salt-finger instability for various R_m. If $B = 10$, for example, one can roughly predict that the stability characteristics of salt-finger

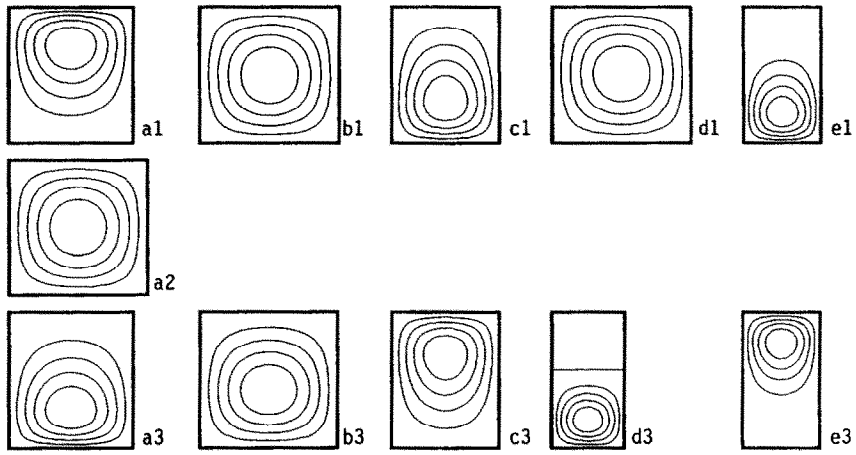

FIG. 7. The streamline patterns in an isotropic and inhomogeneous porous layer at selected values of A, B, and C for $R_m = 1$ and 50. (a1) $A = 1$, $B = C = 0$, $R_m = 1$; (a2) $A = 0$, $B = C = 0$, $R_m = 1$; (a3) $A = -1$, $B = C = 0$, $R_m = 1$; (b1) $B = 1$, $A = C = 0$, $R_m = 1$; (b3) $B = -1$, $A = C = 0$, $R_m = 1$; (c1) $C = 1$, $A = B = 0$, $R_m = 1$; (c3) $C = -1$, $A = B = 0$, $R_m = 1$; (d1) $B = 1$, $A = C = 0$, $R_m = 50$; (d3) $B = -1$, $A = C = 0$, $R_m = 50$; (e1) $C = 1$, $A = B = 0$, $R_m = 50$; (e3) $C = -1$, $A = B = 0$, $R_m = 50$.

convection are very similar to those of thermal convection for a reasonably large range of R_m. When other inhomogeneities come into play, i.e. A and C are non-zero, this figure can also provide valuable information with reasonable accuracy and this will be discussed later.

Again, we summarize the inhomogeneous effects of R_{sm}^c and a_m^c as follows:

1. R_{sm}^c decreases with increasing A whereas a_m^c increases with $|A|$ and is symmetric with respect to $A = 0$.
2. Both R_{sm}^c and a_m^c decrease with increasing B and reach $4\pi^2$ and π, respectively, at B^c, which increases with R_m. For $B \geqslant B^c$, the stability characteristics of salt-finger convection are almost identical with those of thermal convection.
3. R_{sm}^c increases with C, a_m^c increases with $|C|$ and is symmetric with respect to $C = 0$.
4. Larger R_m, in general, results in both larger R_{sm}^c and a_m^c.

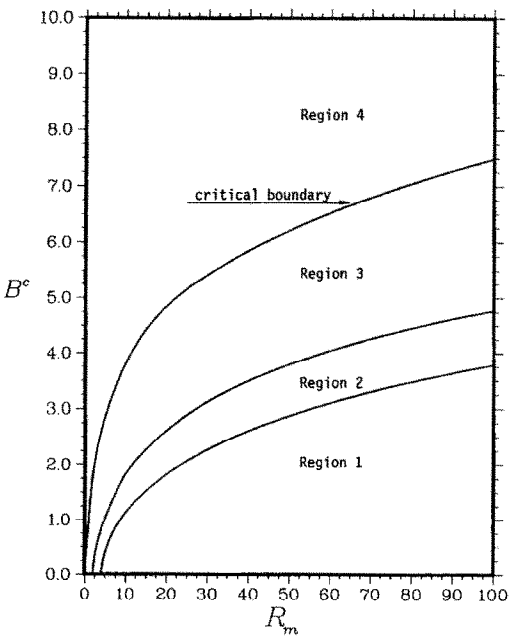

FIG. 8. The critical boundary B^c for various R_m as $A = C = 0$.

As to the cross effect due to inhomogeneities of the porous medium, we present two sets of results for $R_m = 1$ and 50 in Figs. 9 and 10, respectively. For $R_m = 1$ and $B = 0$ (Figs. 9(a1) and (a2)), R_{sm}^c decreases monotonically with increasing A while increases with C, a_m^c increases with A for negative C while decreases for positive C. As $C = 0$, a_m^c increases with $|A|$ and is symmetric with respect to $A = 0$. For the same R_m, but $B = -3$, both the decrease of R_{sm}^c with increasing A and the increase of R_{sm}^c with increasing C are reduced by decreasing B. In other words, the influences of inhomogeneous permeability and solute diffusivity effect are reduced by decreasing B. With regard to a_m^c for decreasing B, except in the case of $C = -5$, the inhomogeneous effects due to permeability and solute diffusivity are also diminished. We also study the case of $R_m = 1$, $B = 3$ and find that the R_{sm}^c and a_m^c differ from those in Figs. 9(a1) and (a2), respectively, by a small amount. It is very difficult, although important, to clearly identify the critical boundary for the cases of A and C being non-zero. We nevertheless present R_{sm}^c and a_m^c in Table 1 for four selected non-zero values of A and C of $R_m = 1$ and 50 in the range $0 \leqslant B \leqslant 10$. It is found that both R_{sm}^c and a_m^c approach constant values at smaller B^c for smaller A and C. Those constants should be the critical values for thermal convection case in the corresponding porous medium. This implication is confirmed by comparing the results of either $R_m = 1$ or

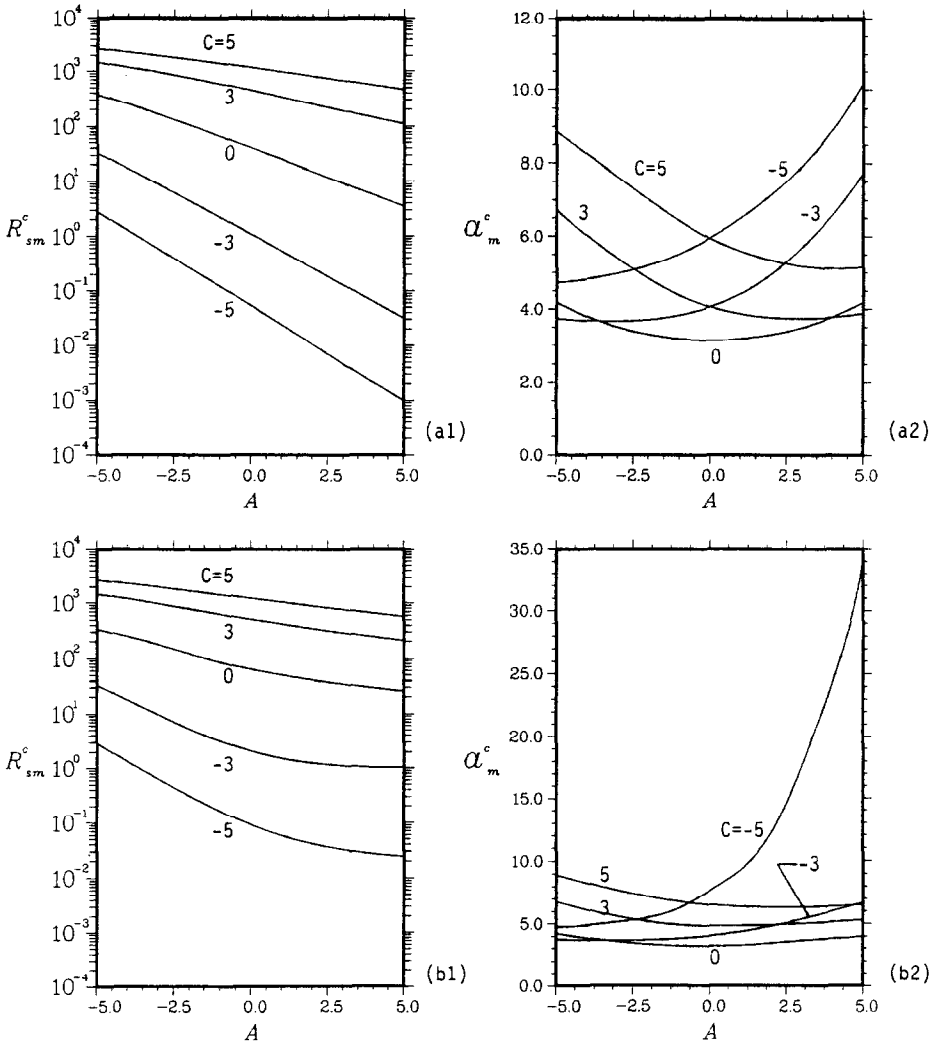

FIG. 9. Cross inhomogeneous effects on the critical conditions for $R_m = 1$. (a1) R^c_{sm} for $B = 0$; (a2) a^c_m for $B = 0$; (b1) R^c_{sm} for $B = -3$; (b2) a^c_m for $B = -3$.

50, $B = 10$ (can be smaller), and $A = C = 1$ and -1 with the corresponding data shown in Figs. 1(a) and (b) of Chen and Hsu [20], from which one can see the comparison is in excellent agreement. That means at sufficient large B, the salt-finger instability characteristics in a porous medium with inhomogeneous permeability and solute diffusivity are identical with those of thermal convection in the same porous medium. As a result, the conclusions made by Chen and Hsu are also applied for the present case as $B > B^c$. In particular, the symmetry of a^c_m with respect to $A = 0$ for $C = 0$, the symmetry between the a^c_m of positive A and B and that of negative A and B, respectively, and the symmetry between the a^c_m of positive A and negative B and that of negative A and positive B still hold.

For $R_m = 50$, the critical conditions for $B = 0$ and 3 are illustrated in Figs. 10(a) and (b), respectively. For $B = 3$, the variation of R^c_{sm} with A (Fig. 10(b1)) is similar to that of $B = 0$, $R_m = 1$ (Fig. 9(a1)) while the a^c_m in Fig. 10(b2) is generally larger than the corresponding a^c_m in Fig. 9(a2), but the variations of a^c_m with A for both cases are still similar. A similar implication applies for the comparisons between Figs. 9(b1) and 10(a1) and between Figs. 9(b2) and 10(a2). We, accordingly, may infer that, for $B < B^c$, the stability characteristics of salt-finger convection for $R_m = 1$ at a certain B are the same with those for $R_m = 50$ at another B. More precisely, the R^c_{sm} and a^c_m for a certain pair of A and C are dependent on a pair of R_m and B; therefore, a critical boundary in terms of R_m and B as shown in Fig. 8 can be obtained for each pair of A and C. Due to the limit of computation resource, to identify the critical boundary for each pair of A and C is a formidable work to the present study. For small A and C, nevertheless, the critical boundary in Fig. 8 ($A = C = 0$) is still valid to some extent.

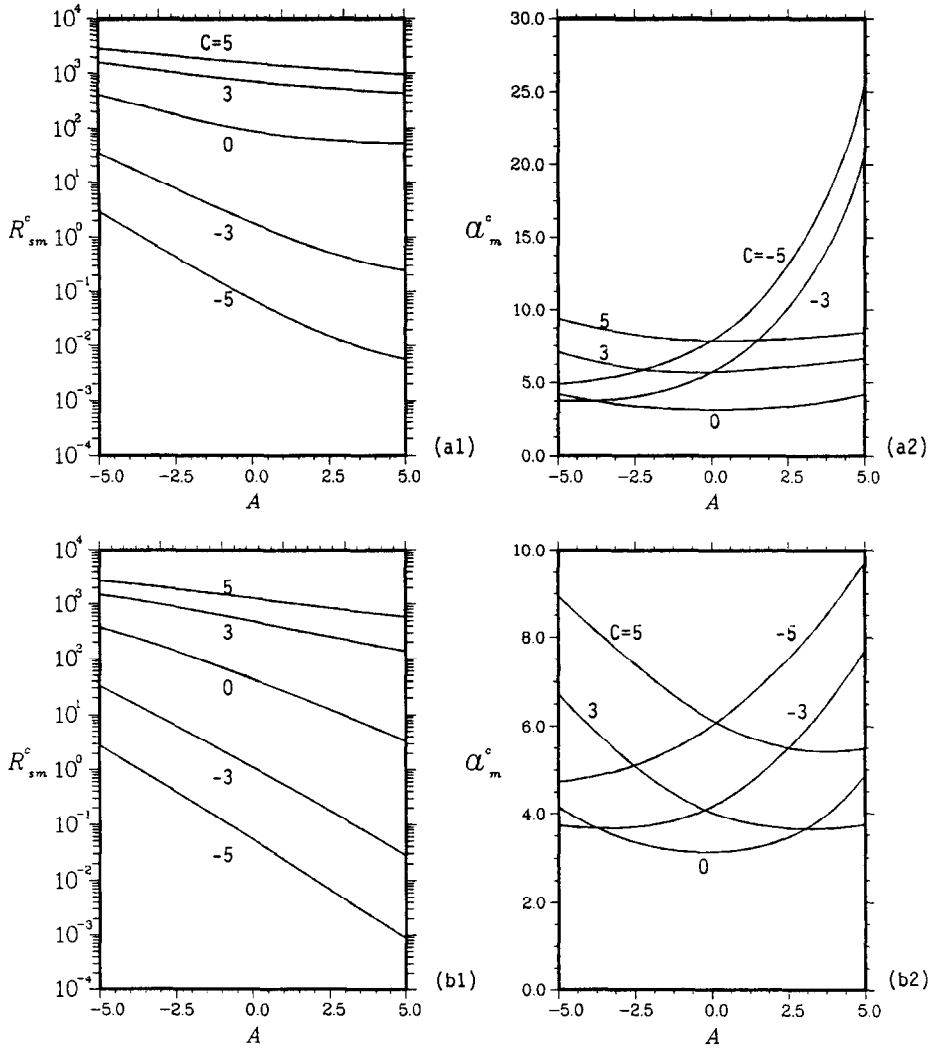

FIG. 10. Cross inhomogeneous effects on the critical conditions for $R_m = 50$. (a1) R^c_{sm} for $B = 0$; (a2) a^c_m for $B = 0$; (b1) R^c_{sm} for $B = 3$; (b2) a^c_m for $B = 3$.

Table 1. The R^c_{sm} and associated a^c_m for $R_m = 1$ and 50 of inhomogeneous porous media

$A = C =$	-3		-1		1		3	
	R^c_{sm}	a^c_m	R^c_{sm}	a^c_m	R^c_{sm}	a^c_m	R^c_{sm}	a^c_m
				$R_m = 1$				
$B = 0$	8.76766	3.66	24.3606	3.20	67.8999	3.20	190.283	3.74
$B = 2$	8.73571	3.66	24.0591	3.20	65.6454	3.19	177.637	3.66
$B = 4$	8.73071	3.65	24.0132	3.20	65.3230	3.20	175.805	3.65
$B = 6$	8.72964	3.65	24.0040	3.20	65.2623	3.20	175.462	3.65
$B = 8$	8.72935	3.65	24.0016	3.20	65.2476	3.20	175.378	3.65
$B = 10$	8.72928	3.65	24.0009	3.20	65.2432	3.20	175.353	3.65
				$R_m = 50$				
$B = 0$	10.4848	3.89	41.6068	3.29	190.144	3.58	518.732	6.19
$B = 2$	9.04328	3.70	26.8413	3.21	85.3222	3.16	287.154	3.94
$B = 4$	8.80325	3.67	24.6243	3.19	69.3134	3.17	198.617	3.61
$B = 6$	8.75121	3.66	24.1751	3.19	66.3236	3.18	181.150	3.62
$B = 8$	8.73710	3.66	24.0601	3.19	65.5968	3.19	177.372	3.64
$B = 10$	8.73241	3.65	24.0244	3.19	65.3787	3.19	176.130	3.64

3.3. *The anisotropic and inhomogeneous porous medium*

Chen and Chen [9] employed the NH_4Cl–H_2O solution as an analog system to examine the critical conditions for the formation of freckles during the directional solidification of concentrated alloys. By using the technique of computed tomography, they identified the vertical porosity distribution in the dendritic mushy zone (Fig. 14 of Chen and Chen [9]). Except the shallow layer close to the interface between the mush and melt, the vertical distribution of porosity of the mushy zone is a linear function

$$\phi(z) = 0.08z + 0.59, \tag{24}$$

where ϕ is the porosity of the porous medium. From the observation of the photos taken in the experiments, they found that the sum of the diameter of primary dendrite arm d_2 and the primary arm space d_1 is approximately 1 mm. The arm space d_1 increases upwards and we may assume its variation in vertical direction is of the form (24). As a result, the averaged d_1 is about 0.63 mm and the averaged d_2 is 0.37 mm. With these measurements, we may compute the physical properties of the mushy zone, which is generally anisotropic and inhomogeneous porous medium.

To determine the vertical and horizontal permeabilities with the measured porosity (24), d_1, and d_2, we use Blake–Kozeny models suggested by Poirier [21]. For vertical permeability,

$$K_3(z) = 1.43 \times 10^{-3} \phi^3(z) d_1^2 / (1 - \phi(z)) \tag{25}$$

is chosen, in which K_3 and d_1^2 are in m^2 and z is dimensionless independent variable, which is 0 at the bottom and 1 at the top. After applying (24) and $d_1 = 0.63$ mm in (25), the averaged value of vertical permeability is about 3.863×10^{-10} m^2. As regards horizontal permeability K_1, we choose [21]

$$K_1(z) = 1.73 \times 10^{-3} \left(\frac{d_1}{d_2}\right)^{1.09} d_2^2 \phi^3(z) (1 - \phi(z))^{-0.749} \tag{26}$$

in which K_1, d_1^2, and d_2^2 are in m^2. The averaged horizontal permeability is thus approximately 2.277×10^{-10} m^2. With these, the anisotropy of permeability is obtained as $\xi = 0.581$, and we take 0.6 for subsequent calculations. We assume the solute diffusivity in the solid of the porous medium is zero so that only the liquid serves to diffuse solute. We thus may imply that $\xi_S = \xi = 0.6$. With regard to ξ_T, we leave it as a free parameter since no existing relation between either ξ and ξ_T or ξ_S and ξ_T is available [18].

The vertical inhomogeneous permeability is shown in (25). By substituting (24) into (25) and after some arrangements, we obtain

$$K_3(z) = 3.63 \times 10^{-12} \times (z + 7.375)^3 / (5.125 - z). \tag{27}$$

Which results in

$$\eta_3(z) = (z + 7.375)^3 / (5.125 - z) \tag{28}$$

and an averaged Darcy number $\delta = K_3^{1/2}(0.5)/d_m = 1.811 \times 10^{-3}$, in which we assume $d_m = 0.01$ m, the depth of the mushy zone corresponding to the onset of plume convection [9]. Similarly, we obtain the horizontal permeability

$$K_1(z) = 1.44 \times 10^{-12} \times (z + 7.375)^3 / (5.125 - z)^{0.749}, \tag{29}$$

and thus

$$\eta_1(z) = (z + 7.375)^3 / (5.125 - z)^{0.749}. \tag{30}$$

Based on the assumption of no solute diffusivity in the solid of the mush, we have $\eta_1(z) = \eta_{S1}(z)$ and $\eta_3(z) = \eta_{S3}(z)$. With regard to inhomogeneous thermal diffusivity, an exponential function as equation (23) is applied. According to Chen and Chen [9], the R_m is small when the plume convection thresholds. We thus take $R_m = 1$ for subsequent calculations.

Based on above measured or estimated values and models, we compute the R_{sm}^c and a_m^c in wide ranges of anisotropy and inhomogeneity of thermal diffusivity,

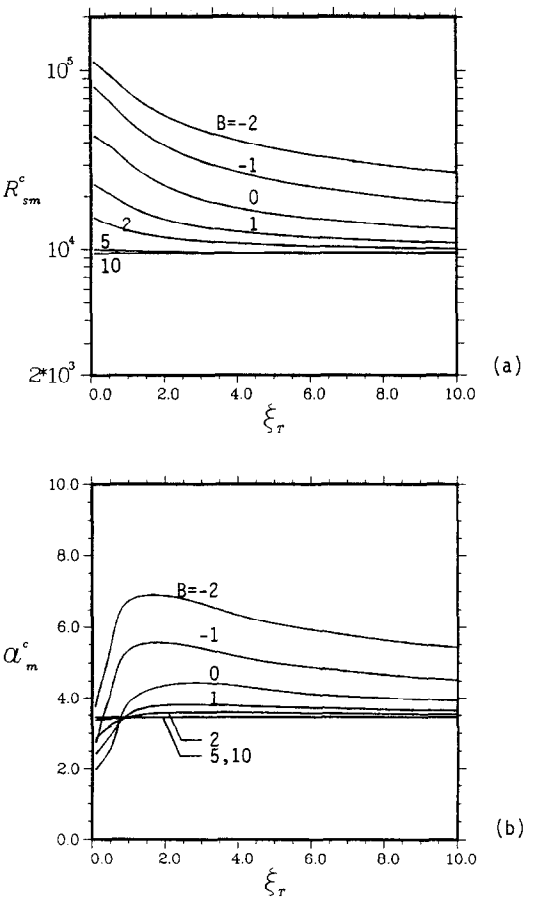

FIG. 11. The critical conditions in an anisotropic and inhomogeneous porous layer $R_m = 1$, $\xi = \xi_S = 0.6$, with $\eta_i(z) = \eta_{Si}(z)$, $i = 1$ and 3 being specified in (28) and (30), respectively. (a) R_{sm}^c; (b) a_m^c.

which cover $0.1 \leqslant \xi_T \leqslant 10$ and $-2 \leqslant B \leqslant 10$, and the results are shown in Figs. 11(a) and (b), respectively. As in previous discussions, R_{sm}^c increases with both decreasing ξ_T and B, a_m^c increases with decreasing B. The effect of ξ_T on a_m^c concluded in Section 3.1, however, holds only for $\xi_T \leqslant 2$ and becomes opposite for $\xi_T \geqslant 2$. This may be due to the inclusion of inhomogeneities of permeability and solute diffusivity; but the proper reason is not yet clear. From Figs. 11, it is seen that R_{sm}^c asymptotically approaches to a value of 9456 and a_m^c to a value of 3.44 as both ξ_T and B increase. It is found that the R_{sm}^c for the onset of salt-finger convection in the porous medium resulted from upward solidifying NH_4Cl–H_2O solution is generally much higher than the R_{sm}^c for the onset of plume convection, which according to the measurement of Chen and Chen [9] is within 200–250. In fact, the thermal diffusivity of the dendritic mushy zone is of finite ξ_T and B. If we consider the dendrites to be of higher thermal diffusivity than the liquid, we may end up with a negative B, say $B = -1$, and a ξ_T is about 1.67 (the inverse of ξ). With these values, the R_{sm}^c can be as high as $O(10^5)$, which results in a much more stable conduction state. Consequently, we may thus draw a tentative conclusion about the relation between the salt-finger and plume convection in the mushy zone that, as the plume is initially ejected from the mush, there is no salt-finger convection in the mush.

In fact, several factors existing in the real solidifying NH_4Cl–H_2O system, such as the solidification in the mush, the moving interface between the melt and mush, the strong salt-finger convection above the mush, and so on, are not considered in the present analysis. Although there is no direct evidence to support that these three factors are not going to dramatically reduce the R_{sm}^c, the following discussion may shed some light on supporting the tentative conclusion. For considering the factor due to the salt-finger convection above the mush, the physical configuration of a porous layer underlying a fluid layer as considered in Chen and Chen [22] can be applied. In the experiment [9], the depth ratio (ratio of the fluid layer depth to the porous layer depth) is found to be always larger than unity (the depth of the fluid layer is determined by the height of the salt-finger convection cell). With this depth ratio, the salt-finger convection is largely confined to the fluid layer and the convection in the porous layer virtually vanishes [22]. This supports our tentative conclusion. As to the influence of moving interface, we do not expect that the R_{sm}^c for salt-finger convection will be substantially diminished by the moving interface since the moving velocity of the interface is much lower than the characteristic convective velocity of salt-finger. For the solidification effect in the mush, the solidifying liquid ejects lighter solution to the mush so that the destabilizing solute gradient is enhanced, thus the R_{sm}^c may be reduced. To our best knowledge, there has been no supportive evidence would show that the deduction of R_{sm}^c due to solidification can be as large as one thousand fold, which would change R_{sm}^c from $O(10^5)$ to $O(10^2)$. In summary, from above discussions, we may infer that the R_{sm}^c with considering the aforementioned factors can be smaller than that of present analysis, but is believed to be larger by several fold than the R_{sm}^c for the plume convection. We thus reach a tentative conclusion that as the plume convection occurs, there is no salt-finger convection in the dendritic mushy zone.

Acknowledgments—The financial support for this work through National Science Council Grant NSC 80-0401-E-002-26 is gratefully acknowledged.

REFERENCES

1. M. E. Glicksman, S. R. Coriell and G. B. McFadden, Interaction of flows with crystal-melt interface, *Ann. Rev. Fluid Mech.* **18,** 307 (1986).
2. H. E. Huppert and M. G. Worster, Dynamic solidification of a binary alloy, *Nature* **314,** 703 (1985).
3. S. M. Copley, A. F. Giamei, S. M. Johnson and M. F. Hornbecker, The origin of freckles in unidirectionally solidified castings, *Metall. Trans.* **1,** 2193 (1970).
4. A. F. Giamei and B. H. Kear, On the nature of freckles in nickel-base superalloys, *Metall. Trans.* **1,** 2185 (1970).
5. K. A. Jackson, J. D. Hunt, D. B. Uhlmann and T. P. Seward, On the origin of the equiaxed zone in castings, *Trans. TMS-AIME* **236,** 149 (1966).
6. R. J. McDonald and J. D. Hunt, Fluid motion through the partially solid regions of a casting and its importance in understanding A-type segregation, *Metall. Trans.* **1,** 1787 (1970).
7. A. K. Sample and A. Hellawell, The mechanism of formation and prevention of channel segregation during alloy solidification, *Metall. Trans. A* **15A,** 2163 (1984).
8. P. H. Roberts and D. E. Loper, Toward a theory of the structure and evolution of a dendrite layer. In *Stellar and Planetary Magnetism* (Edited by A. M. Soward), p. 329. Gordon and Breach, New York (1983).
9. C. F. Chen and F. Chen, Experimental study of directional solidification of aqueous ammonium chloride solution, *J. Fluid Mech.* **227,** 567 (1991).
10. G. Castinel and M. Combarnous, Convection naturelle dans une couche poreuse anisotrope, *Rev. Therm.* **14,** 937 (1975).
11. J. F. Epherre, Critère d'apparition de la convection naturelle dans une couche poreuse anisotrope, *Rev. Therm.* **14,** 949 (1975).
12. R. A. Wooding, Large-scale geothermal field parameters and convection theory, *N.Z. J. Sci.* **21,** 219 (1978).
13. O. Kvernvold and P. A. Tyvand, Nonlinear thermal convection in anisotropic porous media, *J. Fluid Mech.* **90,** 609 (1979).
14. R. McKibbin, Thermal convection in a porous layer: effects of anisotropy and surface boundary conditions, *Transport Porous Media* **1,** 271 (1986).
15. T. Green and R. L. Freehill, Marginal stability in inhomogeneous porous media, *J. Appl. Phys.* **40,** 1759 (1969).
16. D. A. Nield, Onset of thermohaline convection in a porous medium, *Water Resource Res.* **4,** 553 (1968).
17. J. W. Taunton and E. N. Lightfoot, Thermohaline instability and salt fingers in a porous medium, *Phys. Fluids* **15,** 748 (1972).
18. P. A. Tyvand, Thermohaline instability in anisotropic porous media, *Water Resource Res.* **16,** 325 (1980).

19. F. Chen, C. F. Chen and A. J. Pearlstein, Convective instability in superposed fluid and anisotropic porous layers, *Phys. Fluids A* **3,** 556 (1991).
20. F. Chen and L. H. Hsu, Onset of thermal convection in an anisotropic and inhomogeneous porous layer underlying a fluid layer, *J. Appl. Phys.* **69,** 6289 (1991).
21. D. R. Poirier, Permeability for flow of interdendritic liquid in columnar-dendritic alloys, *Metall. Trans. B* **18B,** 245 (1987).
22. F. Chen and C. F. Chen, Onset of finger convection in a horizontal porous layer underlying a fluid layer, *J. Heat Transfer* **110,** 403 (1988).